Cortical and subcortical connections change after repetitive transcranial magnetic stimulation therapy in cocaine use disorder and predict clinical outcome

Jalil Rasgado-Toledo[1+], Victor Issa-Garcia[1,2+], Ruth Alcalá-Lozano[3]*, Eduardo A. Garza-Villarreal[1]*[#], Gabriel González-Escamilla[4]*[#]

+ These authors contributed equally.
# Shared senior authorship

Affiliations

[1] Instituto de Neurobiología, Universidad Nacional Autónoma de México campus Juriquilla, Querétaro, México.
[2] Escuela de Medicina y Ciencias de la Salud TecSalud, Tecnológico de Monterrey, Monterrey, México.
[3] Subdirección de Investigaciones Clínicas, Instituto Nacional de Psiquiatría "Ramón de la Fuente Muñíz", Mexico City, Mexico.
[4] Department of Neurology, Focus Program Translational Neuroscience (FTN), Rhine-Main Neuroscience Network (rmn²), University Medical Center of the Johannes Gutenberg University Mainz, Langenbeckstrasse 1, 55131 Mainz, Germany

*** Corresponding:**

Eduardo A. Garza-Villarreal, MD, PhD
Assistant Professor,
Instituto de Neurobiología, Laboratorio B-03,
Universidad Nacional Autonoma de Mexico (UNAM) campus Juriquilla,
Boulevard Juriquilla 3001,
Santiago de Querétaro, Querétaro, México
C.P. 76230
Phone: (442) 238-1038
Email: egarza@comunidad.unam.mx

Gabriel González-Escamilla, PhD
Department of Neurology, Focus Program Translational Neuroscience (FTN), Rhine-Main Neuroscience Network (rmn²), University Medical Center of the Johannes Gutenberg University Mainz,
Langenbeckstrasse 1, 55131 Mainz, Germany
Tel: +49-6131-177865; email: ggonzale@uni-mainz.de

Ruth Alcalá-Lozano, MD, MSc
Psychiatrist and Clinical Research.
Instituto Nacional de Psiquiatría Ramon de la Fuente Muñiz. Laboratorio de Neuromodulación.
Subdireccion de Investigaciones Clínicas.
Calzada México Xochimilco 101. Colonia San Lorenzo Huipulco, C.P. 14370.
Phone: 5541605065
Email: ruthalcalalozano@gmail.com

Abstract

Background

Cocaine use disorder (CUD) is a worldwide public health condition which is suggested to induce pathological changes in macro- and microstructure. Treatments with psychosocial and pharmacological approaches achieve only low to moderate effects on dealing with cocaine clinical symptomatology. Novel approaches such as repetitive transcranial magnetic stimulation (rTMS) have gained attention to induce a reduction in CUD symptoms, yet its mechanisms remain partially understood. Here, we sought to elucidate whether rTMS induces changes on white matter (WM) microstructure in frontostriatal circuits after two weeks of therapy in patients with CUD, and to test whether baseline WM microstructure of the same circuits has an effect on clinical improvement.

Methods

This study consisted of a 2-week, parallel group, double-blind, randomized controlled clinical trial (acute phase) (sham [n = 23] and active [n = 27]), in which patients received two daily sessions of rTMS on the left dorsolateral prefrontal cortex (lDLPFC) as an add-on treatment. We acquired T1-weighted and HARDI-DWI 2-shell sequences at baseline and at two weeks. To elucidate the effects from active rTMS on frontostriatal WM tracts, we extracted NODDI metrics and performed a linear mixed model. We further evaluated the relationship between clinical outcomes in craving and impulsivity and the baseline white matter microstructure.

Results

After 2 weeks, active rTMS showed a significant increase in neurite density (ICVF or the density of axons and dendrites) compared to sham rTMS in WM tracts connecting left DLPFC with left ($\beta = 0.038$, $d = -0.278$) and right vmPFC ($\beta = 0.034$, $d = -0.112$). Similarly, rTMS showed reduction in orientation dispersion (OD or axon organization) in WM tracts connecting left DLPFC with left caudate nucleus ($\beta = 0.009$, $d = -0.087$), left thalamus ($\beta = 0.006$, $d = -0.489$) and left vmPFC ($\beta = 0.027$, $d = 0.024$). Results also show a greater reduction in craving VAS after 2 weeks rTMS when baseline ICVF was low in WM tracts connecting left caudate nucleus with substantia nigra ($\beta = 22.61$, $d = 0.729$), left pallidum ($\beta = 21.13$, $d = 0.738$), and those connecting left thalamus with substantia nigra ($\beta = 16.30$, $d = 0.649$) and left pallidum ($\beta = 21.92$, $d = 0.723$).

Conclusions

Our results suggest that rTMS induced white matter microstructural changes between fronto-striato-thalamic regions after 2 weeks. rTMS-induced microstructural changes may depend on the baseline integrity of the connections between the striatum, thalamus, and the substantia nigra. Connections that predicted clinical improvement in CUD. The current results support the efficacy of rTMS as a therapeutic tool in the treatment of CUD. However, the individual clinical improvement may rely on each patient's state of structural connections integrity.

Keywords: Cocaine use disorder; Imaging; Transcranial magnetic stimulation; Diffusion MRI; NODDI

Introduction

Cocaine use disorder (CUD) is estimated to affect about 20 million people worldwide (global population age ≥15) (1) and to be one of the leading causes of death in young persons (2), thus it is a public health crisis. CUD is suggested to induce pathological changes in macrostructure and microstructure of the meso-cortico-limbic system in humans and animal models due to the changes in synapses and cells themselves (3), while some studies have shown at least some of these structural changes may be reversible (4,5). Despite the improvement in therapy during recent years for CUD patients, treatments with psychosocial and pharmacological approaches achieve only low to moderate effects on dealing with cocaine clinical symptomatology such as craving, which may lead to a relapse in substance use (6). Nonetheless, novel non-invasive interventions such as repetitive transcranial magnetic stimulation (rTMS) have gained attention by attaining positive outcomes in patients with clinical pathologies, including substance use disorders (SUDs) (7). Although the main mechanisms of rTMS action remain to be fully elucidated, induction of neuroplastic changes on dysregulated circuits through stimulation of cortical structures like dlPFC, rTMS can modulate the function of its connected regions achieving behavioral changes (7,8). In this sense, rTMS may help patients in adequately overcoming symptoms such as craving and impulsivity by producing changes acting at the cellular and genetic circuit level, and rTMS is hypothesized to maintain its clinical effect by means of brain plasticity through long-term potentiation-like and long-term depression-like mechanisms, which may be perceived on MRI as macro- and microstructural changes (8–10). However, to date there is limited evidence on the extent to which rTMS modulates the anatomy of brain circuits in CUD and whether prefrontal rTMS induced microstructural modification that can be related to the clinical outcome either locally or in the connected areas to the stimulation site.

Recent advances in magnetic resonance imaging (MRI) have open new opportunities for the study of microstructural abnormalities, these include the neurite orientation dispersion and density imaging (NODDI) model, which allows to evaluate subtle tissue characteristics by modeling water diffusion within neurites and the free water around them (11). Microstructural characterization with NODDI is possible through the use of different metrics: 1) intra-cellular volume fraction or neurite density index (ICVF), which assesses the density of axons and dendrites, and has been proposed as a sensitive marker for myeloarchitecture and axonal degeneration, 2) isotropic volume fraction (ISOVF) which measures the free water of extracellular compartment as an indirect metric for neuroinflammation, and 3) Orientation dispersion index (OD) which quantifies bending, fanning and the orientational configuration of axons that helps to measure axonal organization (12,13). Within this framework, using NODDI offers a unique opportunity to understand the microstructural plasticity of the human brain as a result of rTMS treatment for CUD. This may be particularly interesting as NODDI can be developed into an indicator of a state-of-disorder and treatment-outcome biomarker, as has been proposed for other diseases (14–18), and described in context of the state-of-disorder for alcohol and cocaine use disorders, however not for treatment-outcome (19,20).

Here, we sought to evaluate whether rTMS induced changes on WM microstructure of frontostriatal circuits after two weeks of therapy and to test whether baseline WM microstructure of the same circuits could predict behavioral responsiveness to rTMS in the same cohort of patients with CUD. To achieve this, we examined the changes in NODDI values after rTMS therapy as well as tested predictions of these over the craving and impulsiveness state.

Methods

Participants

Data was obtained from a clinical trial conducted at the Clinical Research Division of the National Institute of Psychiatry in Mexico City, Mexico that was approved by the Institutional Ethics Research Committee (CEI/C/070/2016) and registered at ClinicalTrials.gov (NCT02986438). During the clinical

trial, patients with cocaine use disorder (CUD) who met the inclusion and did not meet exclusion criteria provided written informed consent to participate, per the Declaration Helsinki. Patients were recruited via flyers on substance use disorder (SUD) clinics and medical institutes in the metropolitan area of Mexico City and through advertisements in social media. The clinical trial consisted of a 2-week, parallel group, double-blind, randomized controlled trial (acute phase) followed by a 6-month open-label trial (maintenance phase). Repetitive transcranial magnetic stimulation (rTMS) was delivered over the left dorsolateral prefrontal cortex (DLPFC) as an add-on to standard treatment. Clinical, behavioral and MRI data was acquired at baseline (T0), 2 weeks (T1), 3 months (T2) and 6 months (T3). The main results of the clinical trial and functional analysis have been published (21). For the purpose of this new study, we focused on the double-blind 2-week acute phase (T0-T1) and the relationship between clinical improvement and white matter structure measured using a novel HARDI-DWI sequence and NODDI analysis. We analyzed 50 participants (sham: 23, active: 27) and the overview of demographic data is shown in **Table 1**. Full methodological details on recruitment, CONSORT flowchart and a complete demographics table, as well as the main study results can be found in our previous publication by Garza-Villarreal et al. (21) and the Supplementary Material.

Behavioral instruments

Table 1 shows descriptive statistics on the scores of the behavioral instruments. A full list of behavioral instruments, their descriptions, and mean scores can be found in Garza-Villarreal et al. (21). Here, we limit to describe the following which were employed in the analyses.

Cocaine Craving Visual Analog Scale (VAS): We designed a VAS to evaluate the participants' craving at the moment of the assessment. The VAS consisted of a continuous 10 cm line (including 2 decimals) in which the left point at 0 cm meant "no craving" and the right point at 10 cm meant "the most intense craving" (22). The participants were asked to mark with a cross the intensity of their craving at the moment of assessment.

Cocaine Craving Questionnaire Now (CCQ-now): The CCQ-Now is a questionnaire containing 45 items that explore cocaine craving at the moment of assessment (23). The items are related to: desire to use cocaine, intention and planning to use cocaine, anticipation of positive outcome, anticipation of relief from withdrawal or dysphoria and lack of control overuse. The higher the score is, the higher current cocaine craving. We employed the CCQ-now Spanish translation which was validated in Mexican population (24).

Barratt Impulsivity Scale Version 11 (BIS-11): The BIS is more than 50 years old (25) and has been extensively revised into the BIS-11 (26). This version of the scale consists of 30 items that describe impulsive and non-impulsive behaviors related to 3 main categories: attentional, motor, and non-planning impulsiveness. The higher the total score is, the higher the impulsivity of the participant. We used the Spanish translation of the BIS-11 (27).

Transcranial magnetic stimulation

During the acute phase, a MagPro R30+Option magnetic stimulator and an eight-shaped B65-A/P coil (MagVenture, Alpharetta, GA) was used to deliver active or sham rTMS over the left DLPFC. The orientation of the coil was anterior-medial and the position was determined using either the 5.5 cm anatomic criterion or the Beam F3 method. Stimulation protocol consisted of 10 weekdays of 2 sessions with 50 trains of 50 pulses at 5 Hz at 100% motor threshold. Each train had a 10-second inter-train interval and each session a 15-minute inter-session interval. A total of 5,000 pulses were delivered per day. For all details on the rTMS protocol please refer to the Supplementary Materials.

Simulation of TMS electrical field

We used SimNIBS (28) version 3.2.3 to perform simulations of the TMS electrical field generated on the participants cortex. We reconstructed head meshes from T1w images using *headreco (29)*. During the study, Brain Navigator was not available, hence, a vitamin E capsule fiducial was used to identify the stimulation target. These scalp coordinates were projected into the cortex and converted to MNI coordinates reported in and with a procedure explained in detail in Garza-Villarreal et al. (21). We converted these MNI coordinates into the native space by using SimNIBS's *mni2subjects_coords* function which were projected back into the scalp before running the subjects' simulations. Simulations were run with the corresponding coordinates, coil orientation (anterior-medial) and 100% motor threshold. For the simulation, we used the MagVenture_MC_B70 coil, since there are no differences in the induced field between the B65-A/P and the MCF-B70 coil. Electric field norms from simulations were mapped into *fsaverage* and then averaged across participants to obtain **Figure 1**.

Magnetic resonance imaging acquisition

T1-weighted (T1w) and DWI-HARDI sequences were acquired using a Philips Ingenia 3T scanner (Philips, USA) with a 32-channel Philips head coil. Parameters of T1w 3D FFE sagittal images were: TR/TE = 7/3.5 ms, FA = 8 degrees, FOV = 240 mm2, matrix = 240 x 240, voxel = 1 x 1 x 1 mm, gap = 0. DWI-HARDI used a spin echo (SE) sequence, TR/TE =9000/127 ms, FOV=230mm2 (for 4 participants=224mm2), matrix=96 x 96 (for 4 participants=112 x 112), number of slices=57 (for 4 participants=58), gap=0, plane=axial, voxel=2.4 x 2.4 x 2.5 mm (for 4 participants=2 x 2 x 2.3 mm), directions: 8 = b0, 32 = b-value 1,000 s/mm2 and 96 = b-value 2,500 s/mm2 (for 4 participants: 96 = b-value 3,000 s/mm2), total = 136 directions. Field maps intended for DWI-HARDI use were acquired using a SE EPI sequence with the following parameters: TR/TE=9000/127ms, flip angle=90°, matrix=128 x 128 (for 4 participants=112 x 112), voxel size=1.8 x 1.8 x 2.5mm (for 4 participants=2 x 2 x 2.3mm), number of slices=57 (for 4 participants=58), phase encoding direction=PA. A total of 7 b0 volumes were acquired.

Preprocessing

T1w preprocessing was performed using FMRIPREP version 1.5.5 (30) [RRID:SCR_016216], a Nipype (31) [RRID:SCR_002502] based tool. Each T1w volume was corrected for INU (intensity non-uniformity) using N4BiasFieldCorrection v2.1.0 (32) and skull-stripped using *antsBrainExtraction.sh* v2.1.0 (using the OASIS template). Brain surfaces were reconstructed using *recon-all* from FreeSurfer v6.0.1 (33) [RRID:SCR_001847], and the brain mask estimated previously was refined with a custom variation of the method to reconcile ANTs-derived and FreeSurfer-derived segmentations of the cortical gray-matter of Mindboggle (34)[RRID:SCR_002438].

DWI-HARDI preprocessing was performed in MRtrix version 3.0_RC3 (35), using a pipeline which included noise removal by principal component analysis (PCA) using the Marchenko-Pastur (MP) universal distribution (36), followed by removal of Gibbs ringing artifacts using the method of local subvoxel-shifts (37). Afterwards, we performed a correction for Eddy currents distortions and motion artifacts via FSL (38). Data was collected with reversed phase-encoded blips, resulting in pairs of images with distortions going in opposite directions (PA). Mean PA field maps were downsampled using FSL *flirt (39–41)* with an identity matrix and trilinear interpolation to match the voxel size of the mean AP b0 from DWI-HARDI images. From these pairs the susceptibility-induced off-resonance field was estimated using a method similar to that described in Andersson *et al. (42)* as implemented in FSL (43) and the two images were combined into a single corrected one. A brain mask was obtained using *dwi2mask (44)* at this point. Finally, a bias field correction was performed (32,45).

Processing

All b0 volumes were extracted from preprocessed HARDI images, which were then averaged into a single mean AP b0 volume. Coregistration of this mean volume from each participant to their anatomical

T1w image was conducted using Freesurfer's *bbregister (41)* to obtain a *.dat* registration file and then to apply it to the preprocessed HARDI image using *mri_vol2vol* with trilinear interpolation and to the brain mask using the same function with nearest neighbor interpolation. We used AMICO's version 1.2.10 (46) implementation of NODDI (13) to fit the model and extract its metrics (ICVF, ISOVF, and OD) within the brain mask voxels.

White matter regions of interest

We chose white matter (WM) regions of interest (ROI) corresponding to frontostriatal circuits based on a reported pathological brain target (21). These circuits connects the following gray matter regions: left dorsolateral prefrontal cortex (DLPFC), left caudate nucleus, substantia nigra, left globus pallidus, left thalamus, left and right ventromedial prefrontal cortex (vmPFC), and right angular gyrus (AngG). To select ROI-coordinates, we used the IIT Human Brain Atlas version 5.0 (47,48) to select the following WM ROIs: **1)** left caudate nucleus and axial section through medulla (the closest in atlas to substantia nigra) (*Caud2Medulla*, label 3785), **2)** left caudate nucleus and left pallidum (*Caud2Palli*, label 3739), **3)** left rostral middle frontal cortex (RMFC, the closest in atlas to left DLPFC) and left caudate nucleus (*DLPFC2Caud*, label 2637), **4)** left RMFC and right medial orbitofrontal cortex (MOC, the closest in atlas to vmPFC) (*DLPFC2rvmPFC*, label 2662), **5)** left RMFC and left thalamus (*DLPFC2Thal*, label 2636), **6)** right inferior parietal cortex (IPC, the closest in atlas to right AngG) and right RMFC (*rAngG2rDLPFC*, label 5675), **7)** left thalamus and axial section through medulla (*Thal2Medulla*, label 3685), **8)** left thalamus and left pallidum (*Thal2Palli*, label 3639), **9)** left MOC and left RMFC (*vmPFC2DLPFC*, label 1326).

For each WM ROI mask, we selected every voxel that was within the top 60 most probable fiber connections passing through that voxel by processing the file *IIT_WM_atlas_256.nii.gz* with *fslmaths*. For WM ROI masks 1 and 7 connecting to substantia nigra (axial section through medulla) an inferior manual deletion of all slices ($Z \leq 87$) was performed using *fsleyes*, since the WM mask extended inferiorly beyond substantia nigra when overlaying over *IITmean_t1_256.nii.gz*. A similar process was performed for WM ROI masks (2 and 8) connecting to globus pallidus to delete all slices ($Z \leq 101$), since the WM mask extended inferiorly beyond globus pallidus.

To registering WM ROI masks into subjects' native spaces, we first performed a coregistration between Freesurfer's *brain.mgz* and *IITmean_t1_256.nii.gz* by using *mri_robust_register (49)* to obtain an LTA registration file. The inverse of the LTA file was then used to warp with *mri_vol2vol* the WM ROI masks into each subject's native space. These masks in native space were then used to obtain the mean NODDI metrics within each WM ROI using R version 4.1.0 and *oro.nifti* version 0.11.0. **Table 1** shows the descriptive statistics of these NODDI metrics across subjects.

Statistical analyses

1) *Changes in NODDI two weeks after rTMS*

Linear mixed-effects models were fitted to elucidate possible effects from active rTMS on frontostriatal WM tracts based on NODDI metrics, while controlling for age and education years. The 27 fitted models were of the following structure:

$$NODDI_{ROI_i} = \beta_0 + \beta_1 \cdot weeks + \beta_2 \cdot rTMS[active] + \beta_3 \cdot age + \beta_4 \cdot education\ years + \beta_5 \cdot weeks \cdot rTMS[active]$$

in which $NODDI_{ROI_i}$ was the ICVF, ISOVF, or OD of each of the 9 WM ROI. Supplementaries tables and figures 1-3 depict the estimates of β_5 from these 27 models.

2) *Baseline NODDI as a predictor of behavioral response to rTMS after two weeks*

To investigate whether baseline NODDI metrics from frontostriatal circuits' WM tracts could predict behavioral response to rTMS, several linear mixed effects models were also fitted. The dependent variable was the behavioral instrument score and the independent variables included the NODDI metric of each of the 9 WM ROI, as shown in the following equation:

$$Score = \beta_0 + \beta_1 \cdot weeks + \beta_2 \cdot NODDI_{ROI_i} + \beta_3 \cdot rTMS[active] + \beta_4 \cdot age + \beta_5 \cdot education\ years + \beta_6 \cdot weeks \cdot NODDI_{ROI_i} + \beta_7 \cdot weeks \cdot rTMS[active] + \beta_8 \cdot NODDI_{ROI_i} \cdot rTMS[active] + \beta_9 \cdot NODDI_{ROI_i} \cdot age + ¿ \beta_{10} \cdot NODDI_{ROI_i} \cdot education\ years + \beta_{11} \cdot weeks \cdot NODDI_{ROI_i} \cdot rTMS[active]$$

in which $Score$ was the score from VAS, CCQ-now, or BIS-11 and $NODDI_{ROI_i}$ same as previously defined. Supplementaries tables and figures 4-12 depict the estimates of β_{11} from these 81 models (3 NODDI metrics *x* 9 WM ROI *x* 3 scores from behavioral instruments).

We corrected p-values using the false discovery rate or FDR method (50) on each of the 12 hypotheses families, each containing the 9 interactions of interest corresponding to the model of each WM ROI. All statistical analyses were calculated using R version 4.1.0. Linear mixed models were performed using *lme4*, *effects*, *lmerTest* libraries, and *emmeans* for Cohen's effect size (d) calculated by estimated marginal means (emm).

Results

Simulation of TMS electrical field

The simulation of the electric field indicated a maximal average electric field norm (111.46 V/m) in the middle frontal gyrus (**Figure 1**).

Changes in NODDI after 2 weeks rTMS

After 2 weeks, active rTMS showed significant increase in neurite density (ICVF or the density of axons and dendrites) compared to Sham rTMS in WM tracts connecting left DLPFC with left vmPFC (p = 0.013, FDR = 0.058, d = -0.278; sham-T1: 0.422 ± 0.135, active-T1: 0.461 ± 0.142) and right (p = 0.009, FDR = 0.058, d = -0.112; sham-T1: 0.451 ± 0.116, active-T1: 0.484 ± 0.126) (**Table 2** and **Figure 2**), though it did not survive multiple comparisons at q = 0.05. Similarly, rTMS showed reduction in orientation dispersion (OD or axon organization) in WM tracts connecting left DLPFC with left caudate nucleus (p = 0.021, FDR = 0.094, d = -0.087; sham-T1: 0.41 ± 0.037, active-T1: 0.416 ± 0.035), left thalamus (p = 0.045, FDR = 0.135, d = -0.489; sham-T1: 0.418 ± 0.03, active-T1: 0.42 ± 0.027), and left vmPFC (p = 0.012, FDR = 0.094, d = 0.024; sham-T1: 0.294 ± 0.095, active-T1: 0.329 ± 0.096), without surviving multiple comparisons either (**Table 2** and **Figure 2**).

Baseline NODDI as a predictor of clinical outcome after rTMS

We found a was greater reduction in craving VAS after 2 weeks rTMS when baseline ICVF was low in WM tracts connecting left caudate nucleus with substantia nigra (p = 0.007, FDR = 0.021, d = 0.729) and left pallidum (p = 0.004, FDR = 0.018, d = 0.738), and those connecting left thalamus with substantia nigra (p = 0.012, FDR = 0.027, d = 0.649) and left pallidum (p = 0.002, FDR = 0.018, d = 0.723) (**Table 3** and **Figure 3A**).

We found that BIS11 responsiveness seemed to be predicted by a high baseline ISOVF or free water in WM connecting DLPFC with left (p = 0.015, FDR = 0.135, d = 1.031) and right (p = 0.038, FDR = 0.171, d = 0.925) vmPFC (**Table 3** and **Figure 3B**). None of these results regarding BIS11 survived multiple comparisons.

Finally, we only found that baseline OD from WM connecting left DLPFC and right vmPFC, when high, predicted greater decrease in BIS11 ($p = 0.020$, FDR = 0.180, $d = 0.827$) (**Table 3** and **Figure 3C**), without surviving multiple comparisons.

Discussion

In this study, we investigated the effects of a 2-week treatment with repeated transcranial magnetic stimulation over the left dorsolateral prefrontal cortex (lDLPFC) on fronto-striato-thalamic white matter (WM) microstructure in cocaine use disorder patients, using longitudinal diffusion weighted imaging. We further evaluated the dependence of clinical changes in craving and impulsivity on baseline white matter microstructure. Our results suggest that rTMS induces WM microstructural changes (density of axons and dendrites, and axon organization) in the left DLPFC-vmPFC and left DLPFC-left caudate nucleus connections after 2 weeks of treatment. We also found that baseline white matter structure predicted clinical response to rTMS treatment.

After 2 weeks of rTMS we evidenced an increase in ICVF and OD, but not ISOVF, in WM tracts connecting the lDLPFC to the ventromedial PFC (vmPFC) and to the left caudate nucleus in the Active group, and a decrease in the Sham group. Although these results did not survive multiple comparisons (FDR at 5%), they show medium effects and therefore shall be considered. These results may suggest firstly, a recovery of the integrity of prefrontal connections neurites due to active rTMS, and secondly, a close-relationship between the fronto-striatal circuits and the dependency behavior. The main mechanism of action proposed for rTMS in SUD treatment is to activate dopamine function in meso-cortico-limbic system and a reinstaining of extracellular glutamate and dopamine concentrations, which could trigger changes of dendritic spine density, neurotransmitter receptor expression, neuronal degeneration, and microglial activation which could explain the microstructural reversive results in basal ganglia and PFC (8,51,52). A previous study has found that rTMS can reach deep subcortical structures such as the amygdala through stimulation of cortical to subcortical connections (53). Our electric-field simulations show that active rTMS in patients with CUD may have reached deep structures reflected by changes in NODDI metrics.

Baseline ICVF of WM tracts connecting left caudate nucleus with substantia nigra and left pallidum, and those connecting left thalamus with substantia nigra and left pallidum frontal and subcortical regions predicted a reduction in craving VAS after the rTMS treatment. These results survived multiple comparisons and were the most robust. This was not the case for ICVF from WM tracts connecting cortical with subcortical regions. On the contrary, ISOVF predicted impulsivity responsiveness in left DLPFC connections to vmPFC and their connection of this to the right DLPFC. Similarly, OD predicted BIS11 responsiveness in one WM ROI. However, these results did not survive multiple comparisons. We suggest that the initial state of WM integrity or the initial topology configuration are important for the rTMS outcome. This may serve as an initial indication to select CUD patients that may more effectively benefit from this therapy.

Previous studies have found associations between repetitive stimulation over the DLPFC as well as the mPFC with improvements in executive functions, reward functions, as well as reduction of craving/drug consumption in patients with CUD (54,55). The prediction of craving outcome based on the state of microstructure prior to stimulations could suggest that greater neurite integrity will result in better rTMS clinical outcomes, which is in line with previous studies that have found associations between gray and white matter baseline integrity with better longitudinal clinical outcomes that can informs if patients will relapse or remain in drug abstinent (56). This idea may be supported by the low effect size we found for NODDI changes, but high for NODDI as predictor. This may imply that irrespective of the induced changes, the initial integrity state has the highest impact on how rTMS modulates brain circuits and on the possible success of clinical outcome.

One of the main limitations of the present work concerns the longitudinal course, which is restricted to a single time point, only after 2 weeks. The results of which could be statistically confirmed with continued use of rTMS in the months of patient follow-up, as well as being extended to other regions. Evenso, finding significant changes at 2 weeks suggests rTMS affects WM structure from the first day of stimulation. According to previous clinical disorders studies, ICVF is decreased with axonal degeneration, axonal loss and demyelination processes while OD decreasing reflects selective loss of crossing fibers, axonal regrowth and reduced axonal dispersion (12). However, other researchers have found apparently contradictory results in terms of NODDI values directionality and the biological interpretation of it (12,16). In this context, validation of NODDI values in terms of biological meaning would help to elucidate the current results. Discussion regarding the clinical sample variability and composition here used can be found in Garza-Villarreal et al. (21).

In conclusion, the here shown reversive neurite microstructure state due to rTMS in connections between the prefrontal cortex and striatum, indicates a plasticity-induced recovery of the integrity of prefrontal connections by active stimulation. The prediction of the craving state based on baseline NODDI values before the onset of rTMS suggests that rTMS efficacy depends on the consumption-related integrity state of the underlying microstructure. Our results highlight rTMS as a potential therapeutic tool in the treatment of CUD, due to its ability to modulate altered brain microstructure by cocaine use, as well as the relevance of NODDI for tracing drug/treatment responsiveness.

Data Availability

The MRI dataset can be found in https://openneuro.org/datasets/ds003037/

Code Availability

For the code analysis presented here, please check: https://jalilrt.github.io/NODDI-changes-by_rTMS-in_CUD/

Acknowledgements

The study was supported by public funds CONACYT FOSISS No. 0260971, CONACYT No. 253072 and PAPIIT-UNAM IA202120. Victor Issa-Garcia and Eduardo A. Garza-Villarreal would like to thank Dirección General de Calidad y Educación en Salud, Secretaría de Salud, México for the scholarship support provided to Victor. We also thank the Laboratorio Nacional de Visualización Científica Avanzada (LAVIS) for the use of their computer cluster and the Laboratorio Nacional de Imagenología por Resonancia Magnética (LANIREM). Gabriel Gonzalez-Escamilla is supported by a grant from the German Research Foundation (DFG; CRC-TR-128). Jalil Rasgado Toledo is a doctoral student from the Programa de Doctorado en Ciencias Biomédicas, Universidad Nacional Autónoma de México (UNAM) and received fellowship 858667 from CONACYT.

References

1. United Nations Office on Drugs and Crime (2022): *World Drug Report 2021 (Set of 5 Booklets)*. United Nations. Retrieved from https://play.google.com/store/books/details?id=LMNdEAAAQBAJ

2. Volkow ND, Koob GF, McLellan AT (2016): Neurobiologic Advances from the Brain Disease Model of Addiction. *N Engl J Med* 374: 363–371.

3. Nestler E (2005): The Neurobiology of Cocaine Addiction. *Science & Practice Perspectives*, vol. 3. pp

4–10.

4. Hirsiger S, Hänggi J, Germann J, Vonmoos M, Preller KH, Engeli EJE, *et al.* (2019): Longitudinal changes in cocaine intake and cognition are linked to cortical thickness adaptations in cocaine users. *Neuroimage Clin* 21: 101652.

5. Hanlon CA, Beveridge TJR, Porrino LJ (2013): Recovering from cocaine: insights from clinical and preclinical investigations. *Neurosci Biobehav Rev* 37: 2037–2046.

6. Kampman KM (2019): The treatment of cocaine use disorder. *Sci Adv* 5: eaax1532.

7. Steele VR, Maxwell AM (2021): Treating cocaine and opioid use disorder with transcranial magnetic stimulation: A path forward. *Pharmacol Biochem Behav* 209: 173240.

8. Moretti J, Rodger J (2022): A little goes a long way: Neurobiological effects of low intensity rTMS and implications for mechanisms of rTMS. *Current Research in Neurobiology* 3: 100033.

9. Ekhtiari H, Tavakoli H, Addolorato G, Baeken C, Bonci A, Campanella S, *et al.* (2019): Transcranial electrical and magnetic stimulation (tES and TMS) for addiction medicine: A consensus paper on the present state of the science and the road ahead. *Neurosci Biobehav Rev* 104: 118–140.

10. Diana M, Raij T, Melis M, Nummenmaa A, Leggio L, Bonci A (2017): Rehabilitating the addicted brain with transcranial magnetic stimulation. *Nat Rev Neurosci* 18: 685–693.

11. Nazeri A, Schifani C, Anderson JAE, Ameis SH, Voineskos AN (2020): In Vivo Imaging of Gray Matter Microstructure in Major Psychiatric Disorders: Opportunities for Clinical Translation. *Biol Psychiatry Cogn Neurosci Neuroimaging* 5: 855–864.

12. Kamiya K, Hori M, Aoki S (2020): NODDI in clinical research. *J Neurosci Methods* 346: 108908.

13. Zhang H, Schneider T, Wheeler-Kingshott CA, Alexander DC (2012): NODDI: practical in vivo neurite orientation dispersion and density imaging of the human brain. *Neuroimage* 61: 1000–1016.

14. Kamagata K, Andica C, Kato A, Saito Y, Uchida W, Hatano T, *et al.* (2021): Diffusion Magnetic Resonance Imaging-Based Biomarkers for Neurodegenerative Diseases. *Int J Mol Sci* 22. https://doi.org/10.3390/ijms22105216

15. Ning L, Rathi Y, Barbour T, Makris N, Camprodon JA (2022): White matter markers and predictors

for subject-specific rTMS response in major depressive disorder. *J Affect Disord* 299: 207–214.

16. Kraguljac NV, Guerreri M, Strickland MJ, Zhang H (2022): Neurite Orientation Dispersion and Density Imaging in Psychiatric Disorders: A Systematic Literature Review and a Technical Note. *Biological Psychiatry Global Open Science*. https://doi.org/10.1016/j.bpsgos.2021.12.012

17. Kraguljac NV, Anthony T, Monroe WS, Skidmore FM, Morgan CJ, White DM, *et al.* (2019): A longitudinal neurite and free water imaging study in patients with a schizophrenia spectrum disorder. *Neuropsychopharmacology* 44: 1932–1939.

18. Favre P, Pauling M, Stout J, Hozer F, Sarrazin S, Abé C, *et al.* (2019): Correction: Widespread white matter microstructural abnormalities in bipolar disorder: evidence from mega- and meta-analyses across 3033 individuals. *Neuropsychopharmacology* 44: 2298.

19. Rasgado-Toledo J, Shah A, Ingalhalikar M, Garza-Villarreal EA (2022): Neurite orientation dispersion and density imaging in cocaine use disorder. *Prog Neuropsychopharmacol Biol Psychiatry* 113: 110474.

20. Morris LS, Dowell NG, Cercignani M, Harrison NA, Voon V (2018): Binge drinking differentially affects cortical and subcortical microstructure. *Addict Biol* 23: 403–411.

21. Garza-Villarreal EA, Alcala-Lozano R, Fernandez-Lozano S, Morelos-Santana E, Dávalos A, Villicaña V, *et al.* (2021): Clinical and Functional Connectivity Outcomes of 5-Hz Repetitive Transcranial Magnetic Stimulation as an Add-on Treatment in Cocaine Use Disorder: A Double-Blind Randomized Controlled Trial. *Biol Psychiatry Cogn Neurosci Neuroimaging* 6: 745–757.

22. Sayette MA, Shiffman S, Tiffany ST, Niaura RS, Martin CS, Schadel WG (2000): The measurement of drug craving. *Addiction*, vol. 95. pp 189–210.

23. Tiffany ST, Singleton E, Haertzen CA, Henningfield JE (1993): The development of a cocaine craving questionnaire. *Drug Alcohol Depend* 34: 19–28.

24. Marín-Navarrete R, Mejía-Cruz D, Templos-Nuñez L, Rosendo-Robles A, González-Zavala M, Nanni-Alvarado R, *et al.* (2011): Validation of a cocaine craving questionnaire (CCQ-G) in Mexican population. *Salud Ment* 34: 491–496.

25. Barratt ES (1959): Anxiety and Impulsiveness Related to Psychomotor Efficiency. *Percept Mot Skills* 9: 191–198.

26. Patton JH, Stanford MS, Barratt ES (1995): Factor structure of the Barratt impulsiveness scale. *J Clin Psychol* 51: 768–774.

27. Oquendo MA, Baca-García E, Graver R, Morales M, Montalvan V, Mann JJ (2001): Spanish adaptation of the Barratt Impulsiveness Scale (BIS-11). *Eur Psychiatry* 15: 147–155.

28. Saturnino GB, Puonti O, Nielsen JD, Antonenko D, Madsen KH, Thielscher A (2019): SimNIBS 2.1: A Comprehensive Pipeline for Individualized Electric Field Modelling for Transcranial Brain Stimulation. In: Makarov S, Horner M, Noetscher G, editors. *Brain and Human Body Modeling: Computational Human Modeling at EMBC 2018*. Cham (CH): Springer. https://doi.org/10.1007/978-3-030-21293-3

29. Nielsen JD, Madsen KH, Puonti O, Siebner HR, Bauer C, Madsen CG, *et al.* (2018): Automatic skull segmentation from MR images for realistic volume conductor models of the head: Assessment of the state-of-the-art. *Neuroimage* 174: 587–598.

30. Esteban O, Markiewicz CJ, Blair RW, Moodie CA, Isik AI, Erramuzpe A, *et al.* (2019): fMRIPrep: a robust preprocessing pipeline for functional MRI. *Nat Methods* 16: 111–116.

31. Gorgolewski K, Burns CD, Madison C, Clark D, Halchenko YO, Waskom ML, Ghosh SS (2011): Nipype: A Flexible, Lightweight and Extensible Neuroimaging Data Processing Framework in Python. *Frontiers in Neuroinformatics*, vol. 5. https://doi.org/10.3389/fninf.2011.00013

32. Tustison NJ, Avants BB, Cook PA, Zheng Y, Egan A, Yushkevich PA, Gee JC (2010): N4ITK: improved N3 bias correction. *IEEE Trans Med Imaging* 29: 1310–1320.

33. Dale AM, Fischl B, Sereno MI (1999): Cortical surface-based analysis. I. Segmentation and surface reconstruction. *Neuroimage* 9: 179–194.

34. Klein A, Ghosh SS, Bao FS, Giard J, Häme Y, Stavsky E, *et al.* (2017): Mindboggling morphometry of human brains. *PLoS Comput Biol* 13: e1005350.

35. Tournier J-D, Smith R, Raffelt D, Tabbara R, Dhollander T, Pietsch M, *et al.* (2019): MRtrix3: A fast,

flexible and open software framework for medical image processing and visualisation. *Neuroimage* 202: 116137.

36. Veraart J, Fieremans E, Novikov DS (2016): Diffusion MRI noise mapping using random matrix theory. *Magn Reson Med* 76: 1582–1593.

37. Kellner E, Dhital B, Kiselev VG, Reisert M (2016): Gibbs-ringing artifact removal based on local subvoxel-shifts. *Magn Reson Med* 76: 1574–1581.

38. Andersson JLR, Sotiropoulos SN (2016): An integrated approach to correction for off-resonance effects and subject movement in diffusion MR imaging. *Neuroimage* 125: 1063–1078.

39. Jenkinson M, Bannister P, Brady M, Smith S (2002): Improved optimization for the robust and accurate linear registration and motion correction of brain images. *Neuroimage* 17: 825–841.

40. Jenkinson M, Smith S (2001): A global optimisation method for robust affine registration of brain images. *Med Image Anal* 5: 143–156.

41. Greve DN, Fischl B (2009): Accurate and robust brain image alignment using boundary-based registration. *Neuroimage* 48: 63–72.

42. Andersson JLR, Skare S, Ashburner J (2003): How to correct susceptibility distortions in spin-echo echo-planar images: application to diffusion tensor imaging. *Neuroimage* 20: 870–888.

43. Smith SM, Jenkinson M, Woolrich MW, Beckmann CF, Behrens TEJ, Johansen-Berg H, *et al.* (2004): Advances in functional and structural MR image analysis and implementation as FSL. *Neuroimage* 23 Suppl 1: S208–19.

44. Dhollander T, Raffelt D, Connelly A (2016): Unsupervised 3-tissue response function estimation from single-shell or multi-shell diffusion MR data without a co-registered T1 image. *ISMRM Workshop on Breaking the Barriers of Diffusion MRI*, vol. 5 5. Retrieved from https://www.researchgate.net/profile/Thijs-Dhollander/publication/307863133_Unsupervised_3-tissue_response_function_estimation_from_single-shell_or_multi-shell_diffusion_MR_data_without_a_co-registered_T1_image/links/57cfb5c708ae83b374623e5a/Unsupervised-3-tissue-response-function-estimation-from-single-shell-or-multi-shell-diffusion-MR-

data-without-a-co-registered-T1-image.pdf

45. Rudrapatna SU, Parker GD, Roberts J, Jones DK (2018): Can we correct for interactions between subject motion and gradient-nonlinearity in diffusion MRI. *Proc. Int. Soc. Mag. Reson. Med*, vol. 1206 1206. Retrieved from https://index.mirasmart.com/ISMRM2018/PDFfiles/1206.html

46. Daducci A, Canales-Rodríguez EJ, Zhang H, Dyrby TB, Alexander DC, Thiran J-P (2015): Accelerated Microstructure Imaging via Convex Optimization (AMICO) from diffusion MRI data. *Neuroimage* 105: 32–44.

47. Zhang S, Arfanakis K (2018): Evaluation of standardized and study-specific diffusion tensor imaging templates of the adult human brain: Template characteristics, spatial normalization accuracy, and detection of small inter-group FA differences. *NeuroImage*, vol. 172. pp 40–50.

48. Qi X, Arfanakis K (2021): Regionconnect: Rapidly extracting standardized brain connectivity information in voxel-wise neuroimaging studies. *Neuroimage* 225: 117462.

49. Reuter M, Rosas HD, Fischl B (2010): Highly accurate inverse consistent registration: a robust approach. *Neuroimage* 53: 1181–1196.

50. Benjamini Y, Hochberg Y (1995): Controlling the False Discovery Rate: A Practical and Powerful Approach to Multiple Testing. *Journal of the Royal Statistical Society: Series B (Methodological)*, vol. 57. pp 289–300.

51. Moretti J, Poh EZ, Rodger J (2020): rTMS-Induced Changes in Glutamatergic and Dopaminergic Systems: Relevance to Cocaine and Methamphetamine Use Disorders. *Frontiers in Neuroscience*, vol. 14. https://doi.org/10.3389/fnins.2020.00137

52. Gay A, Cabe J, De Chazeron I, Lambert C, Defour M, Bhoowabul V, *et al.* (2022): Repetitive Transcranial Magnetic Stimulation (rTMS) as a Promising Treatment for Craving in Stimulant Drugs and Behavioral Addiction: A Meta-Analysis. *J Clin Med Res* 11. https://doi.org/10.3390/jcm11030624

53. Sydnor VJ, Cieslak M, Duprat R, Deluisi J, Flounders MW, Long H, *et al.* (2022): Cortical-subcortical structural connections support transcranial magnetic stimulation engagement of the

amygdala. *Sci Adv* 8: eabn5803.

54. Protasio MIB, Da Silva JPL, Machado S, Chagas SV, Murillo-Rodriguez E, Cruz MS (2019): The Effects of Repetitive Transcranial Magnetic Stimulation in Reducing Cocaine Craving and Use. *Addictive Disorders & Their Treatment*, vol. 18. pp 212–222.

55. Zhang JJQ, Fong KNK, Ouyang R, Siu AMH, Kranz GS (2019): Effects of repetitive transcranial magnetic stimulation (rTMS) on craving and substance consumption in patients with substance dependence: a systematic review and meta-analysis. *Addiction*, vol. 114. pp 2137–2149.

56. Moeller SJ, Paulus MP (2018): Toward biomarkers of the addicted human brain: Using neuroimaging to predict relapse and sustained abstinence in substance use disorder. *Prog Neuropsychopharmacol Biol Psychiatry* 80: 143–154.

Tables

Table 1. Descriptive statistics of demographics, behavioral instruments and NODDI metrics by time point and sham/active groups.

	Sham		**Active**	
	T0 (n = 23)	T1 (n = 20)	T0 (n = 30)	T1 (n = 25)
Demographic				
Sex, n (%)				
Male	20 (87%)	-	25 (83.3%)	-
Female	3 (13%)	-	5 (16.7%)	-
Age in years, mean ± SD	33.3 ± 8.1	-	36.1 ± 6.8	-
Years of education, mean ± SD	13.4 ± 2.8	-	12.9 ± 3.1	-
Behavioral instrument, mean ± SD				
Craving: VAS	2.9 ± 2.9	2.3 ± 2.5	3.7 ± 3.5	1.5 ± 2.4
Craving: CCQ-now	146 ± 47.8	129.2 ± 46.2	148.7 ± 51.5	114.8 ± 44.7
Impulsivity: BIS11	62.6 ± 16.9	59.8 ± 21.4	65 ± 16.6	53.4 ± 17.1
NODDI metrics, mean ± SD	T0 (n = 23)	T1 (n = 20)	(n = 27)	(n = 23)
ICVF: Caud2Medulla	0.812 ± 0.056	0.814 ± 0.063	0.813 ± 0.053	0.825 ± 0.066
ICVF: Caud2Palli	0.818 ± 0.061	0.815 ± 0.066	0.818 ± 0.056	0.823 ± 0.065
ICVF: DLPFC2Caud	0.631 ± 0.076	0.624 ± 0.073	0.627 ± 0.051	0.639 ± 0.063
ICVF: DLPFC2rvmPFC	0.515 ± 0.129	0.477 ± 0.1	0.451 ± 0.116	0.484 ± 0.126
ICVF: DLPFC2Thal	0.676 ± 0.068	0.673 ± 0.071	0.676 ± 0.038	0.686 ± 0.056
ICVF: rAngG2rDLPFC	0.663 ± 0.066	0.668 ± 0.073	0.674 ± 0.036	0.674 ± 0.045
ICVF: Thal2Medulla	0.757 ± 0.08	0.761 ± 0.081	0.759 ± 0.06	0.773 ± 0.072
ICVF: Thal2Palli	0.771 ± 0.067	0.775 ± 0.07	0.776 ± 0.058	0.784 ± 0.066
ICVF: vmPFC2DLPFC	0.476 ± 0.126	0.441 ± 0.1	0.422 ± 0.135	0.461 ± 0.142
ISOVF: Caud2Medulla	0.298 ± 0.068	0.296 ± 0.077	0.336 ± 0.072	0.333 ± 0.085
ISOVF: Caud2Palli	0.212 ± 0.064	0.214 ± 0.07	0.247 ± 0.067	0.249 ± 0.076
ISOVF: DLPFC2Caud	0.178 ± 0.057	0.175 ± 0.059	0.192 ± 0.042	0.192 ± 0.04
ISOVF: DLPFC2rvmPFC	0.288 ± 0.078	0.287 ± 0.086	0.281 ± 0.084	0.283 ± 0.086
ISOVF: DLPFC2Thal	0.219 ± 0.055	0.217 ± 0.061	0.242 ± 0.046	0.242 ± 0.05
ISOVF: rAngG2rDLPFC	0.143 ± 0.038	0.149 ± 0.043	0.164 ± 0.032	0.163 ± 0.035
ISOVF: Thal2Medulla	0.393 ± 0.09	0.388 ± 0.101	0.434 ± 0.071	0.431 ± 0.081
ISOVF: Thal2Palli	0.313 ± 0.079	0.313 ± 0.086	0.348 ± 0.075	0.349 ± 0.082

ISOVF: vmPFC2DLPFC	0.144 ± 0.047	0.139 ± 0.049	0.138 ± 0.048	0.147 ± 0.049
OD: Caud2Medulla	0.378 ± 0.041	0.373 ± 0.047	0.398 ± 0.044	0.393 ± 0.052
OD: Caud2Palli	0.355 ± 0.028	0.351 ± 0.028	0.362 ± 0.033	0.362 ± 0.037
OD: DLPFC2Caud	0.423 ± 0.041	0.411 ± 0.031	0.41 ± 0.037	0.416 ± 0.035
OD: DLPFC2rvmPFC	0.399 ± 0.073	0.391 ± 0.083	0.365 ± 0.093	0.381 ± 0.094
OD: DLPFC2Thal	0.421 ± 0.037	0.411 ± 0.03	0.418 ± 0.03	0.42 ± 0.027
OD: rAngG2rDLPFC	0.415 ± 0.024	0.405 ± 0.019	0.413 ± 0.027	0.411 ± 0.024
OD: Thal2Medulla	0.429 ± 0.064	0.423 ± 0.072	0.455 ± 0.049	0.446 ± 0.053
OD: Thal2Palli	0.413 ± 0.04	0.407 ± 0.044	0.426 ± 0.034	0.423 ± 0.037
OD: vmPFC2DLPFC	0.347 ± 0.093	0.327 ± 0.089	0.294 ± 0.095	0.329 ± 0.096

Mean (standard deviation) for demographics and NODDI metrics for each tract: n = sample size, T0 = baseline, T1 = after 2 week; ICVF = intra-cellular volume fraction, ISOVF = isotropic volume fraction, OD = Orientation dispersion: WM-ROI tracts.

Table 2. Coefficients of linear mixed effects models' interaction (weeks:rTMS[active]) showing the effect of rTMS on NODDI metrics from frontostriatal circuits' white matter (WM) tracts.

WM ROI	Estimate	Std. error	df	Effect size	p-value	FDR*
Neurite density (ICVF)						
DLPFC2rvmPFC	0.034	0.012	42.36	-0.112	0.009*	0.058
vmPFC2DLPFC	0.038	0.015	42.31	-0.278	0.013*	0.058
Orientation dispersion (OD)						
DLPFC2Caud	0.009	0.004	40.65	-0.087	0.021*	0.094
DLPFC2Thal	0.006	0.003	40.68	-0.489	0.045*	0.135
vmPFC2DLPFC	0.027	0.010	41.91	0.024	0.012*	0.094

$$NODDI_{ROI_i} = \beta_0 + \beta_1 \cdot weeks + \beta_2 \cdot rTMS[active] + \beta_3 \cdot age + \beta_4 \cdot education\ years + \beta_5 \cdot weeks \cdot rTMS[active]$$

DLPFC2Caud: WM connecting left rostral middle frontal cortex (RMFC) and left caudate nucleus, DLPFC2rvmPFC: WM connecting left RMFC and right medial orbitofrontal cortex (MOC), DLPFC2Thal: WM connecting left RMFC and left thalamus, vmPFC2DLPFC: WM connecting left MOC and left RMFC. *False discovery rate (FDR) adjustment was implemented with p-values of their own metric, full values are found in supplementaries tables 1-3.

Table 3. Coefficients of linear mixed effects models' 3-way interaction (weeks:NODDI:rTMS[active]) predicting decrease in craving VAS/total BIS11 using baseline NODDI metrics from frontostriatal circuits' WM tracts.

WM ROI	Estimate	Std. error	df	Effect size	p-value	FDR*
ICVF | Cocaine Craving Visual Analog Scale (VAS)						
Caud2Medulla	22.61	7.93	40.12	0.729	0.007*	0.021*
Caud2Palli	21.13	6.95	40.17	0.738	0.004*	0.018*
Thal2Medulla	16.30	6.17	40.07	0.649	0.012*	0.027*

Thal2Palli	21.92	6.61	40.13	0.723	0.002*	0.018*
ISOVF | Barratt Impulsivity Scale Version 11 (total BIS-11)						
DLPFC2rvmPFC	-49.81	23.25	39.63	1.031	0.038*	0.171
vmPFC2DLPFC	-103.78	40.96	40.51	0.925	0.015*	0.135
OD | Barratt Impulsivity Scale Version 11 (total BIS-11)						
DLPFC2rvmPFC	-56.76	23.43	39.80	0.827	0.020*	0.180

$$Score = \beta_0 + \beta_1 \cdot weeks + \beta_2 \cdot NODDI_{ROI_i} + \beta_3 \cdot rTMS[active] + \beta_4 \cdot age + \beta_5 \cdot education\ years + \beta_6 \cdot weeks \cdot NODDI_{ROI_i} + \beta_7 \cdot weeks \cdot rTMS[active] + \beta_8 \cdot NODDI_{ROI_i} \cdot rTMS[active] + \beta_9 \cdot NODDI_{ROI_i} \cdot age + ¿ \beta_{10} \cdot NODDI_{ROI_i} \cdot education\ years + \beta_{11} \cdot weeks \cdot NODDI_{ROI_i} \cdot rTMS[active]$$

Caud2Medulla: WM connecting left caudate nucleus and axial section through medulla, Caud2Palli: WM connecting left caudate nucleus and left pallidum, DLPFC2rvmPFC: WM connecting left rostral middle frontal cortex (RMFC) and right medial orbitofrontal cortex (MOC), Thal2Medulla: WM connecting left thalamus and axial section through medulla, Thal2Palli: WM connecting left thalamus and left pallidum, vmPFC2DLPFC: WM connecting left MOC and left RMFC. *False discovery rate (FDR) adjustment was implemented with p-values of their own metric, full values are found in supplementaries tables 4-12.

Figures

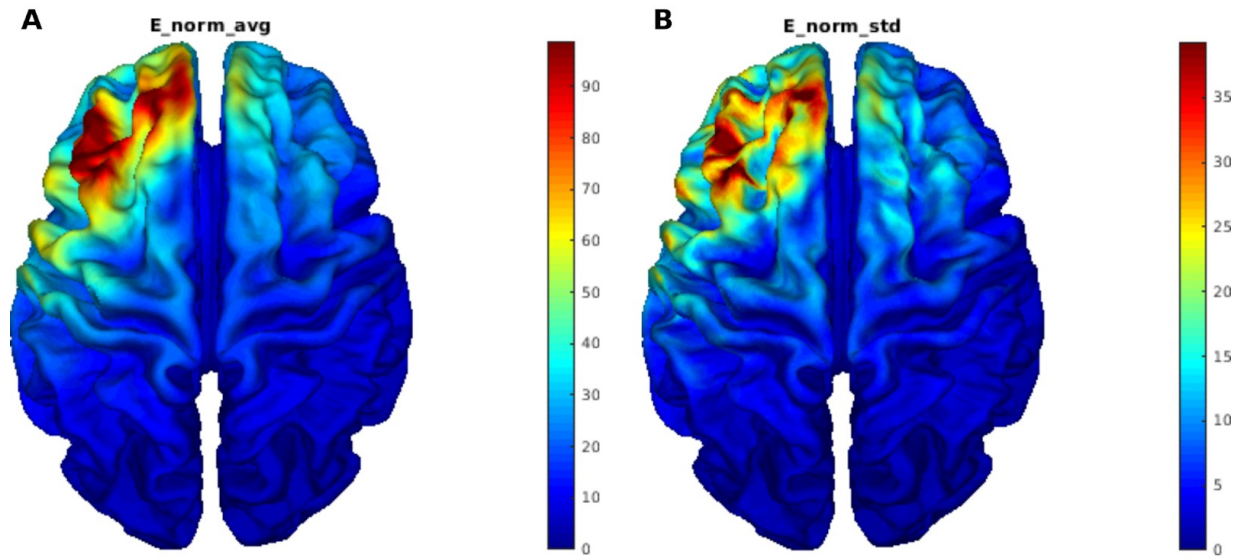

Figure 1. Visualization of A) mean (V/m) and B) standard deviation (V/m) of electric field norms from simulations across subjects.

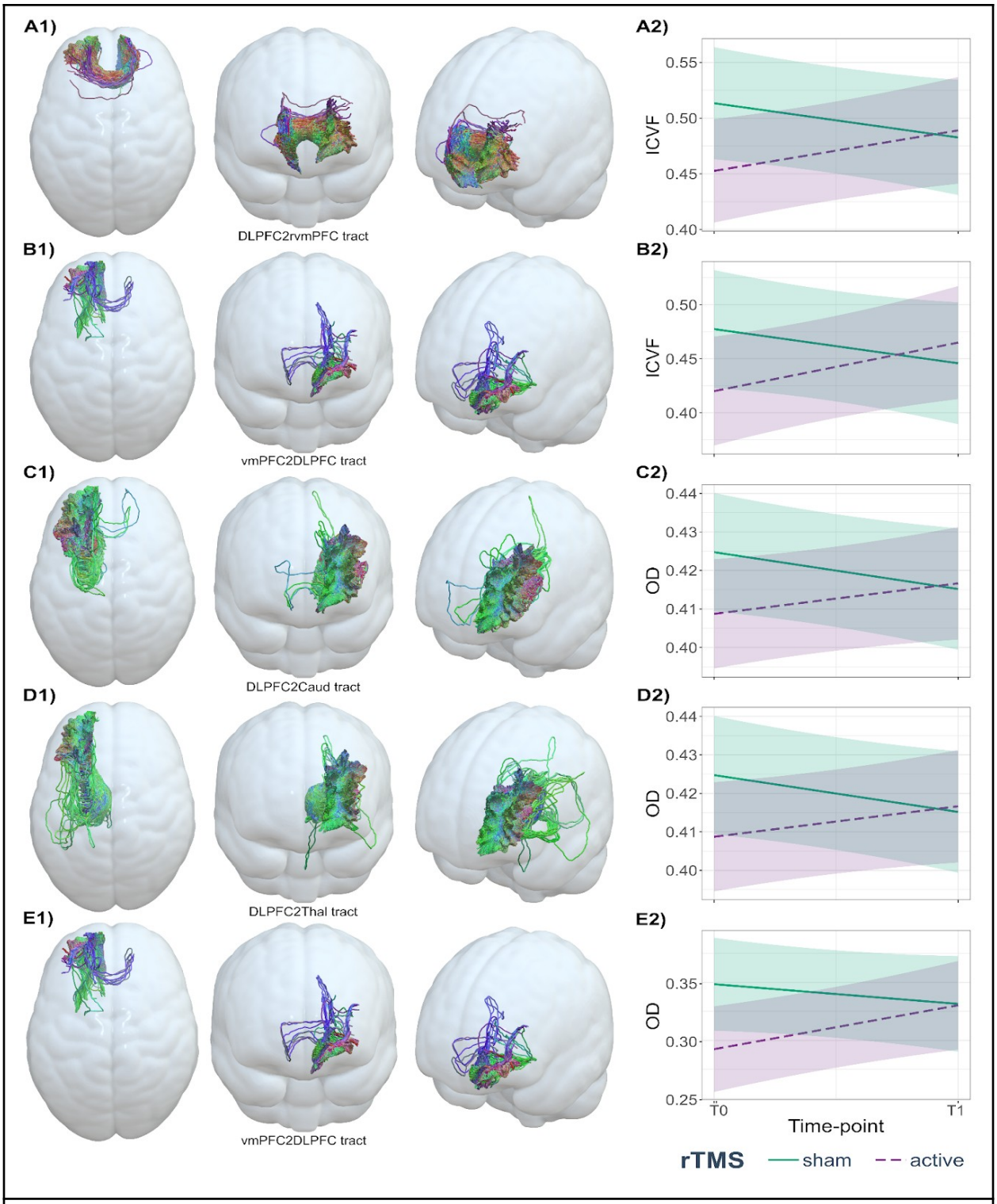

Figure 2. Effect of rTMS on neurite density (ICVF) and orientation dispersion (OD) from frontostriatal circuits' WM tracts. A2) Mean ICVF values at baseline and after two weeks of the white matter connecting the left rostral middle frontal cortex and right medial orbitofrontal cortex (A1: DLPFC2rvmPFC), B2) Mean ICVF values at baseline and after two weeks of the white matter

connecting left medial orbitofrontal cortex and left rostral middle frontal cortex (B1: vmPFC2DLPFC), C2) Mean OD values at baseline and after two weeks of the white matter connecting left rostral middle frontal cortex and left caudate nucleus (C1: DLPFC2Caud), D2) Mean OD values at baseline and after two weeks of the white matter connecting left rostral middle frontal cortex and left thalamus (D1: DLPFC2Thal), E2) Mean OD values at baseline and after two weeks of the white matter connecting left medial orbitofrontal cortex and left rostral middle frontal cortex (E1: vmPFC2DLPFC).

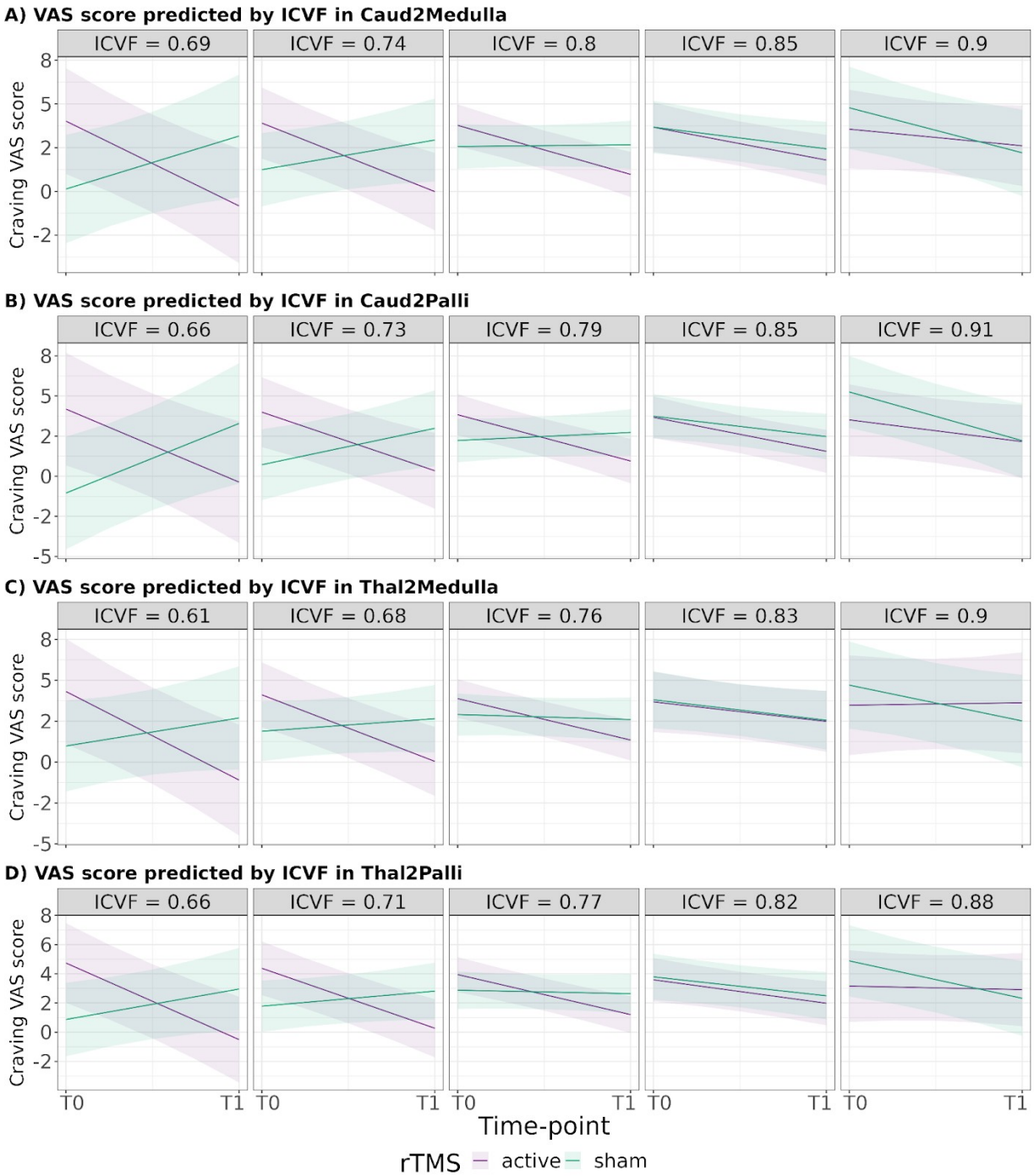

Figure 3. Prediction of craving VAS scores by the effect of rTMS on ICVF from frontostriatal circuits' WM tracts. A) prediction of craving VAS scores from different ICVF values in WM connecting left caudate nucleus and axial section through medulla (Caud2Medulla), B) prediction of craving VAS scores from different ICVF values in WM connecting left caudate nucleus and left pallidum (Caud2Palli), C) prediction of craving VAS scores from different ICVF values in WM connecting left thalamus and axial section through medulla (Thal2Medulla), D) prediction of craving VAS scores from

different ICVF values in WM connecting left thalamus and left pallidum (Thal2Palli). VAS = craving Visual Analog Scale, ICVF = neurite density index, T0 = baseline time-point, T1 = after two weeks of rTMS protocol.

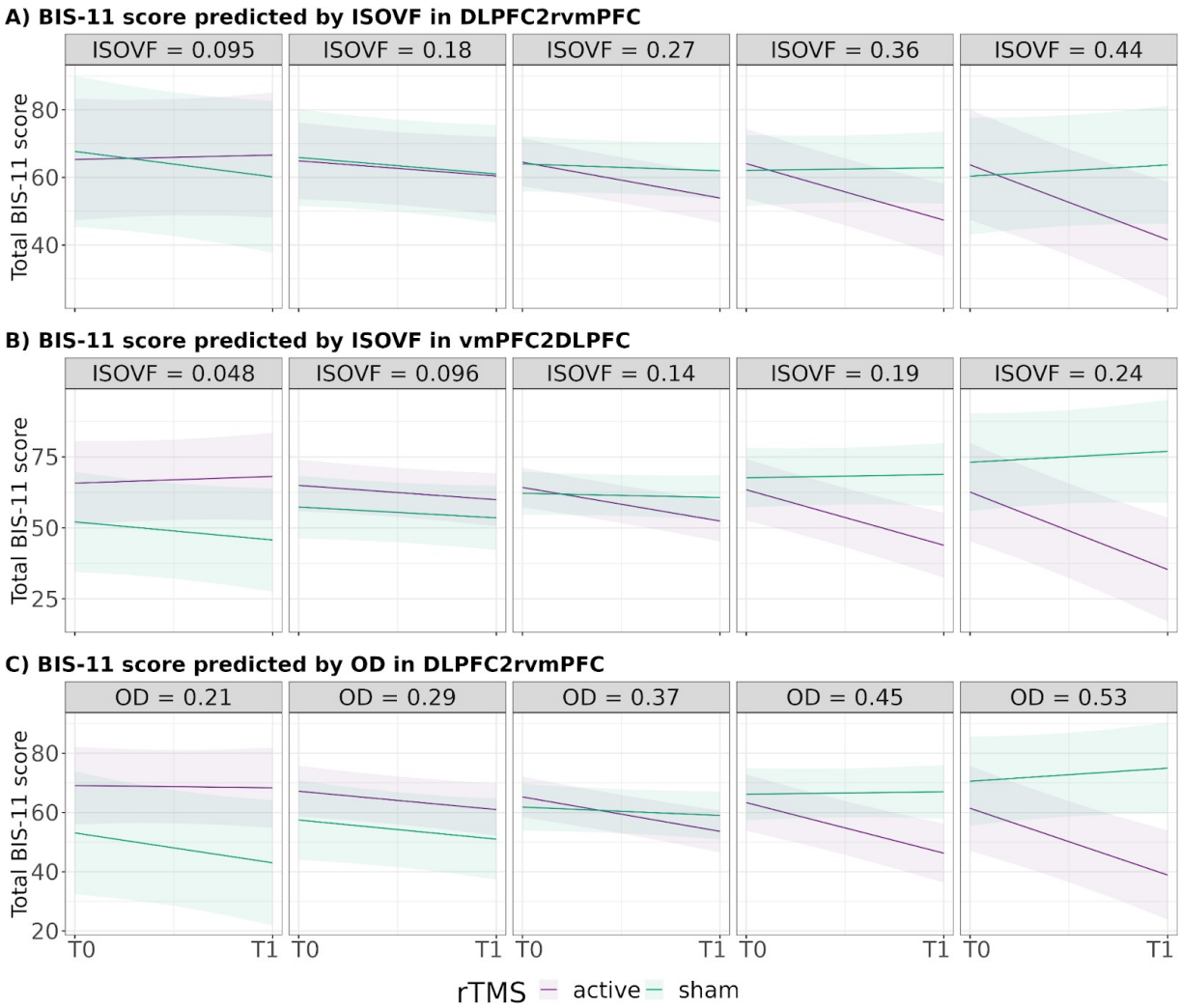

Figure 4. Prediction of total BIS-11 scores by the effect of rTMS on ISOVF/OD from frontostriatal circuits' WM tracts. A) prediction of total BIS-11 scores from different ISOVF values in WM connecting left rostral middle frontal cortex and right medial orbitofrontal cortex (DLPFC2rvmPFC), B) prediction of total BIS-11 scores from different ISOVF values in WM connecting left right medial orbitofrontal cortex and left left rostral middle frontal cortex (vmPFC2DLPFC), C) prediction of total BIS-11 scores from different OD values in DLPFC2rvmPFC. BIS-11 = Barratt Impulsivity Scale v. 11, ISOVF = CSF volume fraction, OD = orientation dispersion, T0 = baseline time-point, T1 = after two weeks of rTMS protocol.